Available online at www.sciencedirect.com
SCIENCE DIRECT®
Journal of Sound and Vibration 273 (2004) 637–651
JOURNAL OF SOUND AND VIBRATION
www.elsevier.com/locate/jsvi

Measuring high-frequency wave propagation in railroad tracks by joint time–frequency analysis

F. Lanza di Scalea*, J. McNamara

Department of Structural Engineering, University of California, San Diego, 9500 Gilman Drive, M.C. 0085, La Jolla, CA 92093-0085, USA

Received 16 July 2002; accepted 28 April 2003

Abstract

The behavior of high-frequency elastic waves propagating in railroad tracks is relevant to the field of rail noise generation and long-range rail inspection. While a large amount of theoretical and numerical work exists to predict transient vibrations propagating in rails, obtaining experimental data has been particularly challenging due to the multimode and dispersive behavior of the waves.

In this work a joint time–frequency analysis based on the Gabor wavelet transform is employed for characterizing longitudinal, lateral and vertical vibrational modes propagating in rails in the 1000–7000 Hz range. The Gabor transform optimizes the time–frequency resolution of the measurements and theoretically requires a single excitation point and a single measurement point. These features make the analysis well-suited for the study of wave propagation in rails.

The theory of the wavelet transform is reviewed in the context of dispersive measurements. Accelerometer data were taken from a section of rail subject to impulse dynamic testing in the laboratory. The group (energy) velocity dispersion curves and the frequency-dependent attenuation of the waves were successfully extracted from the wavelet scalograms of the accelerometer signals.

1. Introduction

Knowledge of the vibration characteristics of railroad tracks is critical to predicting the noise generated by a passing train (wheel/rail noise) as well as in the context of rail defect detection by long-range inspection. In analogy with beam vibrations, the known vibrational modes of railroad tracks in the 100–7000 Hz range can be identified as longitudinal (axial)

*Corresponding author. Tel.: +1-858-822-1458; fax: +1-858-534-6373.
E-mail address: flanza@ucsd.edu (F. Lanza di Scalea).

0022-460X/03/$ - see front matter
doi:10.1016/S0022-460X(03)00563-7

modes, lateral modes and vertical modes [1,2]. These vibrations are generally characterized by complex deformation patterns involving cross-sectional deformations of the rail that make simple beam vibration models inapplicable, particularly above 1500 Hz. A common feature is that the displacement of the rail head is dominant at lower frequencies, while cantilever bending of the rail foot becomes significant at higher frequencies (nominally above 3000 Hz).

While advanced theoretical and numerical models have been developed for predicting the behavior of transient rail vibrations [1–6], experimental studies are particularly challenging due to the multimode (multiple modes propagating at the same frequency) and dispersive (propagation velocities depending on frequency) characteristics of the propagating waves. Classical Fourier transform techniques cannot be used in multimode and dispersive wave propagation cases. This is the reason why experimental studies of wave propagation in rails have been seldom attempted. An impulse hammer excitation with accelerometer detection was employed in Ref. [7], where the propagation velocities of vertical and lateral rail vibrations were successfully isolated in the field at various frequencies. The method used in Ref. [7], like the 2-D Fourier transform method [8], requires multiple, equally spaced measurement (or excitation) points that limit the practicality of the technique. In addition, limitations to the highest measurable frequency (5000 Hz in Ref. [7]) and to the maximum number of measurable modes are imposed by the spacing of the measurement points and by the number of the measurement cross-sections.

As an alternative to techniques that use waveforms from multiple, equally spaced measurements, joint time–frequency methods that require only a single signal are gaining increasing attention for the analysis of multimode and dispersive waves. The wavelet transform (WT) is one powerful joint time–frequency analysis technique.

A known fact when sampling dynamic signals is that a sufficiently wide time window is required to appropriately characterize low-frequency components. Conversely, a narrow time window is appropriate to characterize high-frequency components. This means that a constant time window cannot maintain adequate resolution in the low-frequency and in the high-frequency ranges simultaneously, that is the main disadvantage of the short-time Fourier transform (STFT). When compared to the STFT, the WT has a multiresolution capability deriving from a flexible window that is broader in time for observing low frequencies and shorter in time for observing high frequencies [9]. This feature results in high resolution in time as well as in frequency. When compared to the pseudo-Wigner–Ville distribution (PWVD), that also optimizes the time–frequency resolution, the WT does not generate signal cross-terms that can be detrimental when multiple echoes occur [10]. In the field of wave propagation, the multiresolution capabilities of the WT have been successfully exploited for the study of flexural waves in beams [9,11,12], guided waves in plates and in thin films [13–15] and for the localization of acoustic emission sources [16].

This paper shows that the WT can be successfully utilized to measure high-frequency waves propagating in rail tracks including longitudinal, lateral and vertical vibrational modes at frequencies as high as 7000 Hz. The results presented were obtained from a rail section tested in the laboratory by impulse hammer excitation and accelerometer detection. The signals were analyzed in terms of group (energy) velocity–frequency relationship and frequency-dependent attenuation.

2. The wavelet transform

The wavelet transform (WT) of a function $f(t)$ can be written as [17]

$$Wf(u,s) = \int_{-\infty}^{+\infty} f(t)\frac{1}{\sqrt{s}}\psi^*\left(\frac{t-u}{s}\right)\mathrm{d}t, \tag{1}$$

where $\psi^*(t)$ is the complex conjugate of the mother wavelet function $\psi(t)$ defined as

$$\psi_{u,s}(t) = \frac{1}{\sqrt{s}}\psi\left(\frac{t-u}{s}\right). \tag{2}$$

The mother wavelet can be considered as a window function in the time and in the frequency domains where u is known as the translation parameter and s as the scaling parameter. As indicated in Eq. (2), u shifts the wavelet in time and s controls the wavelet frequency bandwidth. The flexible window provides multiresolution capability to the WT thus optimizing the time–frequency resolution of the analysis.

The mother wavelet function must satisfy the admissibility condition

$$\int_{-\infty}^{+\infty}\frac{|\hat{\psi}(\omega)|^2}{|\omega|}\mathrm{d}\omega < \infty, \tag{3}$$

where ω is the angular frequency and $\hat{\psi}(\omega)$ is the Fourier transform of $\psi(t)$. The admissibility condition imposes that $\psi(t)$ has zero average such that

$$\int_{-\infty}^{+\infty}\psi(t)\,\mathrm{d}t = 0. \tag{4}$$

An analytic wavelet can be created by modulating the frequency of a real and symmetric window $g(t)$ as follows:

$$\psi(t) = g(t)\exp(\mathrm{i}\eta t). \tag{5}$$

The Fourier transform of $\psi(t)$ in Eq. (5) is $\hat{\psi}(\omega) = \hat{g}(\omega-\eta)$ with a center frequency of η.

According to the Heisenberg uncertainty principle, a signal cannot be fully resolved both in time and in frequency simultaneously. The time–frequency resolution of the signal depends on the time–frequency resolution of the analyzing wavelet $\psi_{u,s}(t)$ [17]. Each time–frequency window $\psi_{u,s}(t)$ can be represented by a Heisenberg box centered on the frequency axis at η/s and on the time axis at u. The sides of the Heisenberg box are of lengths σ_ω/s and $s\sigma_t$ where σ_ω is the spread of the wavelet window in frequency and σ_t is the spread of the wavelet window in time. The uncertainty principle implies that the area of the Heisenberg box must be lower bounded by 0.5, that is $\sigma_t\sigma_\omega \geqslant 0.5$.

In this study the Gabor wavelet transform (GWT) is chosen because it provides the best balance between time resolution and frequency resolution since it uses the smallest possible Heisenberg uncertainty box ($\sigma_t\sigma_\omega = 0.5$) [17]. In the case of the Gabor wavelet, $g(t)$ is a Gaussian window defined as

$$g(t) = \frac{1}{\sqrt[4]{(\sigma^2\pi)}}\exp\left(\frac{-t^2}{2\,\sigma^2}\right) = \frac{1}{\sqrt[4]{\pi}}\sqrt{\frac{\eta}{G_s}}\exp\left(\frac{-(\eta/G_s)^2t^2}{2}\right), \tag{6}$$

where η is the wavelet center frequency, σ is the standard deviation of the Gaussian window, and $G_s = \sigma\eta$ is known as the Gabor shaping factor.

The choice of η and G_s influences the time–frequency resolution of the analysis. As commonly done in joint time–frequency studies of wave propagation [9,11,14,16], the Gabor wavelet center frequency used here is 2π. Since the signal angular frequency ω is given by η/s, choosing $\eta = 2\pi$ conveniently sets the inverse of the scaling parameter equal to the frequency, that is $1/s = f = \omega/2\pi$.

As for the G_s parameter, while the *product* of the time resolution and the frequency resolution (area of the Heisenberg box) is kept at the best possible value of 0.5 with the Gabor wavelet, the choice of the factor G_s (and therefore σ, for fixed η) selects the *relative* resolution achievable in time and in frequency (*shape* of the Heisenberg box). For example, decreasing G_s decreases the achievable time resolution while increasing the frequency resolution.

The optimum value of G_s must be chosen on the basis of the particular application. Although theoretically any value of $G_s \gg 1$ will satisfy the admissibility condition equation (3), it has been found in practice that G_s cannot have a value lower than 3.5 [12]. Most authors use $G_s = 5.336$ for dispersive wave propagation studies [9,11,14,16]. The choice of this values of G_s in the present paper will be further justified on the basis of a pilot experiment discussed in Section 3 involving flexural vibrations in cylindrical waveguides. The Gabor wavelet with $\eta = 2\pi$ and $G_s = 5.336$ is plotted in Fig. 1 in the time and in the frequency domains.

The energy density spectrum of a WT, defined as $P_{wf}(u,s) = |Wf(u,s)|^2$ and commonly referred to as a scalogram, indicates the energy of signal $f(t)$ in the Heisenberg box of each wavelet window $\psi_{u,s}(t)$ around time $t = u$ and angular frequency $\omega = \eta/s$. The scalogram is often normalized by the scaling parameter. In this case it is referred to as the normalized scalogram $P_{wf}(u,s)/s$. Besides providing the time–frequency information of the signal components, the scalogram retains the signal energy content. It is therefore possible to extract both the dispersion curves and the frequency-dependent attenuation.

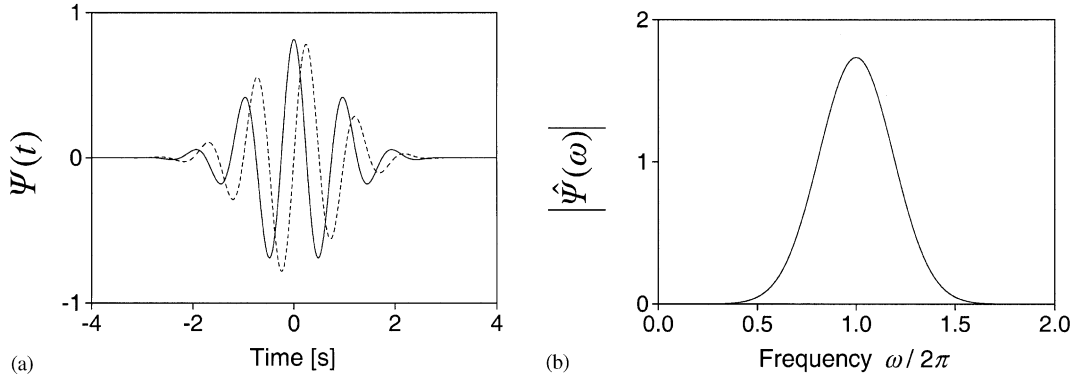

Fig. 1. The Gabor wavelet with $\eta = 2\pi$ and $G_s = 5.336$. (a) Time domain : —-, real component; - - - - -, imaginary component. (b) Magnitude of Fourier spectrum.

3. Pilot test: flexural waves in a cylindrical waveguide

The effectiveness of the GWT for dispersion measurements was first assessed in the case of a slender, isotropic cylindrical waveguide for which well-established, theoretical solutions exist. In particular, the role of the Gabor shaping factor G_s was investigated for the lowest order flexural mode.

Following the formulation of Ref. [18], the Pochhammer–Chree frequency equation describing elastic waves in a cylindrical waveguide of radius r can be written as

$$\begin{vmatrix} \beta^2 - 1 - (qr)^2 \dfrac{v-1}{2v-1} & \beta^2 - 1 - (qr)^2 & 2(\beta^2-1)\varphi_\beta(qr) - (qr)^2 \\ -1 & v\varphi_\beta(qr) - 1 & \beta^2 - 2\varphi_\beta(qr) - (qr)^2 \\ \varphi_\beta(pr) & (1-v)\varphi_\beta(qr) & \beta^2 \end{vmatrix} = 0, \tag{7}$$

where $p^2 = (\omega/c_L)^2 - k^2$; $q^2 = (\omega/c_T)^2 - k^2$; $v = 0.5(\omega/kc_T)^2$; $\varphi_\beta(pr) = (pr)\mathrm{J}'_\beta(pr)/\mathrm{J}_\beta(pr)$; $\varphi_\beta(qr) = (qr)\mathrm{J}'_\beta(qr)/\mathrm{J}_\beta(qr)$; c_L and c_T are the bulk longitudinal and shear wave velocities, respectively; $\omega = 2\pi f$ is the angular frequency; k is the wavenumber; J_β is a Bessel function of order β and $\mathrm{J}'_\beta(x) = 0.5[\mathrm{J}_{\beta-1}(x) - \mathrm{J}_{\beta+1}(x)]$.

The lowest order flexural mode, typically referred to as $F(1,1)$, is obtained from Eq. (7) for $\beta = 1$. For a given vibrational mode, Eq. (7) predicts one or more real values of k for a given ω. The group (energy) velocity dispersion curves, $c_g(f)$, can be directly found from equation (7) considering that $c_g = \mathrm{d}\omega/\mathrm{d}k$.

The experiments were conducted on a steel rod having a diameter of 31.75 mm and a length of 1060 mm. One end of the rod was struck transversely by an instrumented impulse hammer and the propagating signal was detected at the opposite end by an accelerometer (flat frequency response from 0 Hz to about 15 kHz). The accelerometer sensitive axis was along the rod radial direction so as to detect flexural waves. The group velocity was measured at the various frequencies by considering the difference in arrival times between the first arrival (propagating across one rod length) and the first echo (propagating across three rod lengths). The arrival times were identified at each frequency from the GWT scalogram of the recorded time waveforms. The group-velocity extraction procedure is discussed in more detail in Section 4.2 when presenting the rail tests.

The experimental results are presented in Fig. 2(a) for three different values of G_s used for the analyzing wavelet. The center frequency η was kept constant at 2π. The three values examined are $G_s = 3.5$, 5.336 and 8.0. The theoretical solution from Eq. (7) is also presented in Fig. 2(a) with $c_L = 5.8$ km/s and $c_T = 3.2$ km/s for steel. The discrepancies between experimental and theoretical results are plotted in Fig. 2(b) in terms of relative percentage mismatch. This quantity is defined as $[(E - T)/T] \times 100$ where E is an experimental value and T the corresponding theoretical prediction. These mismatches are caused by the finite time–frequency resolution inherently associated to the uncertainty principle. From Fig. 2(b), the average relative mismatch (in absolute value) over the entire frequency range 800–10 500 Hz is measured at 5.31% for $G_s = 3.5$, 3.3% for $G_s = 5.336$ and 5.1% for $G_s = 8.0$. The value of $G_s = 5.336$ is therefore the best compromise between frequency and time resolutions in this test. It is also clear from the figure that the mismatch tends to increase at the lower frequencies, due to the larger size of the wavelet time window required by the Heisenberg principle. Below 1700 Hz, the average relative

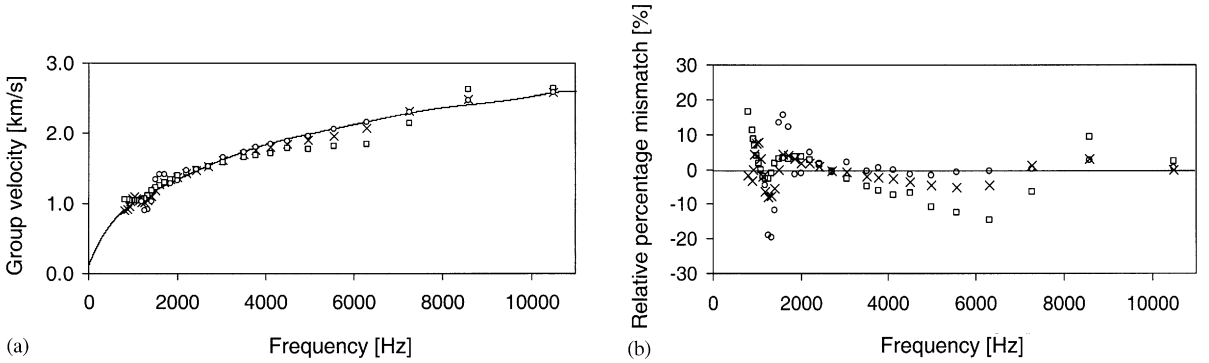

Fig. 2. Group velocity dispersion curve for the lowest order flexural mode in a steel rod. (a) Measured by Gabor wavelet transform with $\eta = 2\pi$: □, $G_s = 3.5$; ×, $G_s = 5.336$; ○, $G_s = 8.0$; —-, from Pochhammer–Chree theory. (b) Relative percentage mismatch between measurements and theory.

mismatch is measured at 4.5% for $G_s = 3.5$, 4.1% for $G_s = 5.336$ and 13.7% for $G_s = 8.0$. The intermediate value of $G_s = 5.336$ is still the best choice.

4. Rail testing

4.1. Experimental set-up

Dynamic testing was conducted on a 4.6 m long section of a 115 lb/yard American Railway Engineering Association (AREA) tee rail. The test section was donated by the San Diego Trolley, Inc. company. The rail was laid in the laboratory on wooden sleepers with a 0.61 m (2 ft) spacing with steel pads and no fasteners. The same instrumented impulse hammer used for the rod test was employed to excite a broadband signal at one end of the rail. The same accelerometer (flat frequency response from 0 Hz to about 15 kHz) was employed to detect the vibrations propagating to the other end of the rail.

As schematized in Fig. 3, longitudinal (axial) vibrational modes were examined by exciting and detecting the waves longitudinally (Fig. 3(a)); lateral and vertical vibrational modes were examined by exciting and detecting the waves transversely and vertically, respectively (Figs. 3(b) and 3(c)). Signal excitation and detection were performed at the opposite ends of the rail where no sleepers were placed so as to limit damping at these cross-sections. While excitation was always performed at the rail head, detection was attempted at the rail head and the rail foot in all of the test configurations examined. Foot signals yielded an acceptable signal-to-noise ratio (SNR) only in the case of the vertical vibrations (Fig. 3(c)) at frequencies above 2200 Hz. For the longitudinal and the lateral tests the displacement of the rail head was large enough in the 1000–7000 Hz frequency range examined.

The smallest frequency value that can be properly analyzed by the WT is directly related to the total number of points used when sampling the signal [17]. The present study used a sampling rate of 1 MHz for a maximum recording time of 0.01 s. This sampling rate was appropriate to capture

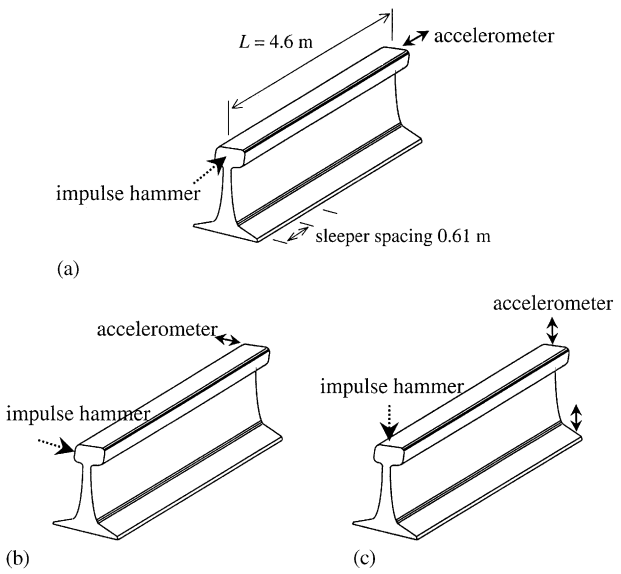

Fig. 3. Experimental set-up for the study of (a) longitudinal, (b) lateral and (c) vertical vibrations propagating in rails.

the largest frequency expected. The recording time was such that only the first arrival and the first echo were recorded. The lower-bound frequency value of 1000 Hz in the WT analysis was dictated by these digitization constraints. The upper-bound value of 7000 Hz resulted from the poor SNR of the measurements beyond this limit (typical SNR ~ 1 dB for the longitudinal wave at 7000 Hz). This limitation derived primarily from the -30 dB roll-off of the hammer excitation signal beyond 7000 Hz.

For the extraction of group velocity values and attenuation values as a function of frequency, the accelerometer signals were analyzed by comparing the first detected arrival (propagation across one rail length) with the first detected echo (propagation across three rail lengths). This dual measurement scheme is often used in wave propagation studies, particularly when an echo signal is available from the free end of the structure under investigation. The main advantage for the measurement of wave velocities and attenuation is that the results are not dependent on the characteristics of the excitation signal. The hammer used in this study typically produced a pulse with a duration of 0.25 ms and a frequency response with a -6 dB roll-off at 3000 Hz. The finite pulse duration would introduce an uncertainty in the measured velocity if a single detected signal were used. The uncertainty would also be dependent on the particular trigger level used for the acquisition. Similarly, the finite bandwidth of the hammer signal would make it difficult to determine directly the frequency-dependent attenuation with a single detection. Another advantage of the dual detection scheme is that the propagation length being probed is doubled when compared to a single detection (two rail lengths against one rail length). The extraction of wave velocity and attenuation is carried out over a larger distance thereby increasing the accuracy of the measurements.

The only known rail vibrational modes that were not successfully identified in the present study are the torsional mode and the two higher order lateral mixed modes predicted in previous

analyses [2,4]. Different arrangements for the signal excitation and detection may be required for these cases.

4.2. Results: wavelet scalograms

Representative time histories recorded by the accelerometer for the longitudinal, the lateral and the vertical vibrations are presented in Figs. 4(a), 5(a) and 6(a) respectively. These signals were all detected at the rail head. The dispersive nature of the waves is evident in the plots. The corresponding GWT normalized scalograms in the frequency range 1000–7000 Hz are presented below the time histories in Figs. 4(b), 5(b) and 6(b). The three scalograms clearly indicate the first arrival of the wave packets after travelling for one rail length and the first echo that has propagated three times the rail length. The different shape of the wavelet contours corresponding to the first arrivals and to the echoes is due to the wave dispersion and frequency-dependent attenuation phenomena.

The scalogram in Fig. 4(b) for the longitudinal test shows an additional wave packet that is centered at around 6000 Hz with arrival time of about 3.5 ms. This signal is identified as the first arrival of one of the higher order longitudinal modes that are known to exist in rails above 5000 Hz [2]. Higher order modes will be discussed more extensively in Sections 4.3 and 4.4. Successful identification of this additional mode is a classical example of the effectiveness of the WT time–frequency analysis of multimode signals.

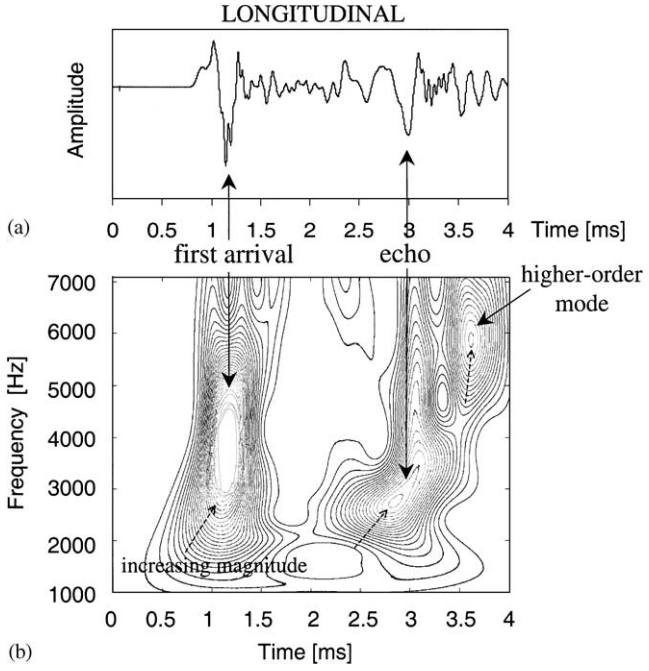

Fig. 4. (a) Recorded longitudinal vibrations in the time domain. (b) Normalized Gabor wavelet scalogram of trace (a) (contour plot).

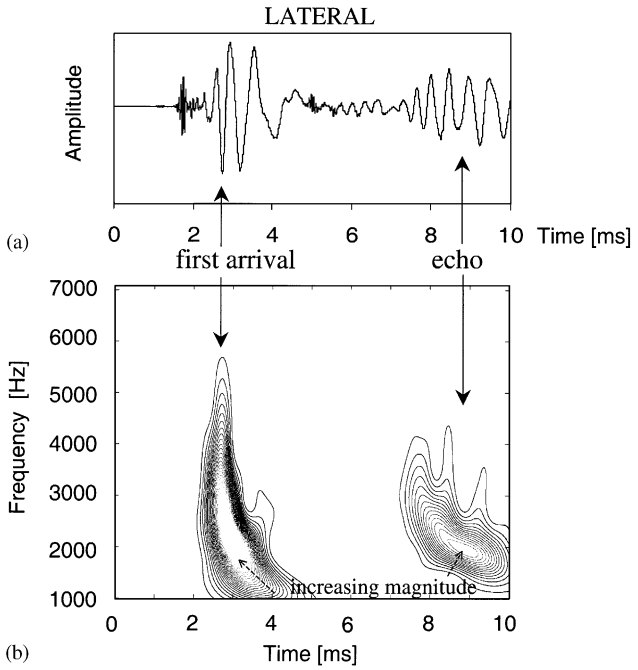

Fig. 5. (a) Recorded lateral vibrations in the time domain. (b) Normalized Gabor wavelet scalogram of trace (a) (contour plot).

The time–frequency information contained in the normalized scalograms can be used to determine the group velocity dispersion curves and the frequency-dependent attenuation curves. One important point is that since the scalogram is a map of the energy of the signal, it is the wave group (energy) velocity that is measured, rather than the wave phase velocity. The line profile plot in Fig. 6(c) demonstrates the extraction procedure for the vertical wave at a frequency of 2000 Hz. At each frequency value, the time difference between the first arrival and the echo is directly related to the wave group velocity through the known length of the rail. This step involves a peak finding numerical routine to extract the arrival times of the wave packets with largest energy (ridges of the scalogram). The group velocity can be expressed as

$$c_g(f) = \frac{2L}{t_2(f) - t_1(f)}, \tag{8}$$

where L is the length of the rail, $t(f)$ is the arrival time of the GWT scalogram ridge at the frequency f, and the subscripts 1 and 2 refer to the first arrival and the echo respectively.

Similarly, the energy of the first arrival relative to that of the echo is related to the wave attenuation. A linear attenuation coefficient $\alpha(f)$ expressed as decibel per meter of propagation length can be defined as

$$\alpha(f)(\mathrm{dB/m}) = \frac{10\log[A_1(f)/A_2(f)]}{2L}, \tag{9}$$

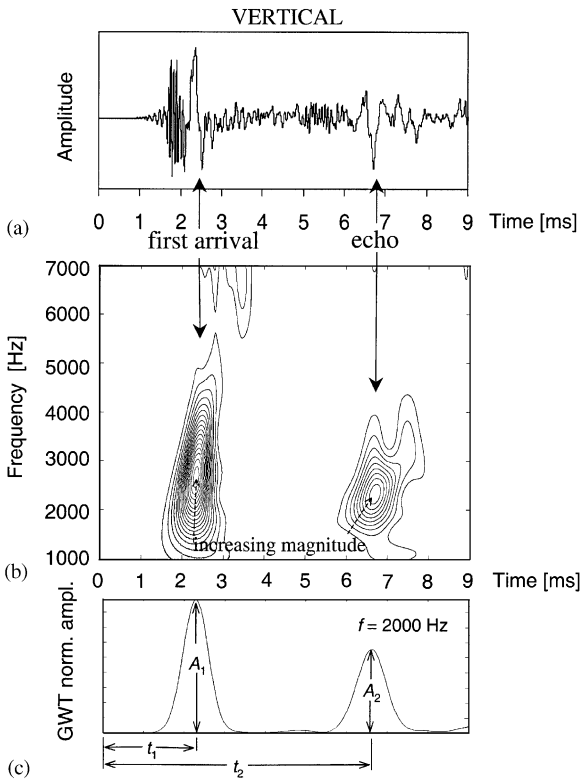

Fig. 6. (a) Recorded vertical vibrations in the time domain. (b) Normalized Gabor wavelet scalogram of trace (a) (contour plot). (c) Line profile of scalogram at $f = 2000$ Hz showing procedure to extract group velocity and attenuation values.

where $A(f)$ is the magnitude of the scalogram ridge at the frequency f, the subscripts 1 and 2 still refer to the first arrival and the echo, respectively, and L is expressed in m. The quantity in Eq. (9) is sometimes referred to as decay rate.

4.3. Group velocity dispersion curves

Fig. 7 shows the group velocity dispersion curves for the longitudinal, the lateral and the vertical vibrational modes obtained from the corresponding GWT scalograms. For comparison, the plots include the velocity values obtained by the classical finite element analysis of rail vibrations in Ref. [2] that examined a UIC861-3 rail. Ref. [2] presents the dispersion results in terms of wavenumber (k) versus frequency (f). The known relation $c_g = 2\pi\, \mathrm{d}f/\mathrm{d}k$ was applied for the group velocity representation used in Fig. 7.

The plots in Fig. 7(a) show that three longitudinal modes were successfully identified as predicted by previous analyses [2,3]. It should be noted that the two higher-order modes are sometimes referred to as "vertical" vibrations [3] due to the dominant foot flapping displacements. Since it is the non-negligible axial head displacement that was detected in the

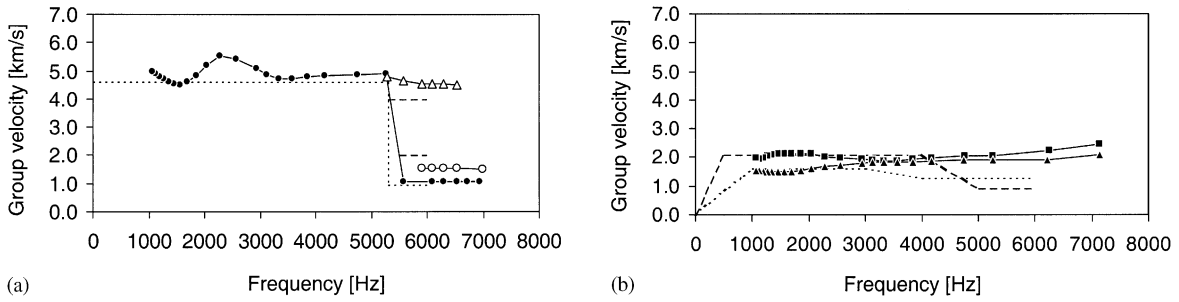

Fig. 7. (a) Group velocity dispersion curves for the longitudinal modes: ●, lowest order mode L0; △, higher order mode L1; ○, higher order mode L2; - - - - -, theoretical results by Gavric in Ref. [2] for mode L0; – –, theoretical results in Ref. [2] for modes L1 and L2. (b) Group velocity dispersion curves for the lateral and for the vertical modes: ▩, vertical mode; ▲, lateral mode; – –, theoretical results in Ref. [2] for vertical mode; - - - - -, theoretical results in Ref. [2] for lateral mode.

tests presented, these modes are here called "longitudinal" following the notation in Ref. [2]. The overall behavior of the measured modes is qualitatively similar to the predictions of Ref. [2]. Perfect matching was not expected because the geometry of the UIC861-3 rail used in the analysis is slightly different from that of the 115 lb/yard AREA rail tested in the laboratory.

The lowest order longitudinal mode, L0 (denominated $ax1$ in Ref. [2]), propagates at an average group velocity of around 5 km/s up to 5200 Hz and slows down to 1 km/s above 5200 Hz. For steel, with nominal modulus $E = 210$ GPa and density $\rho = 7800$ kg/m^3, the longitudinal velocity in a rod in the low frequency × diameter region (bar velocity) is $\mathrm{sqrt}(E/\rho) = 5.2$ km/s. This value matches well with the average velocity measured in Fig. 7(a) at low frequencies. The first of the higher order modes, L1 ($ax2$ in Ref. [2]), cuts on at 5300 Hz and propagates dispersively at velocities above 4 km/s. The second higher order mode, L2 ($ax3$ in Ref. [2]), cuts on at 5900 Hz and propagates at 1.5 km/s with negligible dispersion.

One noticeable feature of the experimental results in Fig. 7(a) is that L0 exhibits some dispersion in the low frequency range (1000–3000 Hz). Dispersion is not expected in the predictions of Ref. [2] for the dominant longitudinal mode below 5000 Hz. No other experimental results for this particular mode below 4500 Hz seem to exist in the open literature. It could be argued that the measured dispersion is the result of inaccuracies in the determination of the arrival times from the GWT scalogram. However, the finite time window of the wavelet used here is adequately small to properly represent the dispersive signals. A simple simulation test was carried out to demonstrate this point. A short, non-dispersive pulse (0.3 ms duration) was simulated in the time domain as shown in Fig. 8(a). A finite impulse response (FIR) digital notch filter was applied to the short pulse to investigate any role of frequency-dependent attenuation on the apparent dispersion measurements. The specific filter used a notch frequency of 1760 Hz with a −3.5 dB stopband bandwidth of 800 Hz and zero phase distorsion. The filtered pulse is shown in the same Fig. 8(a) delayed by ~2 ms from the unfiltered pulse. The GWT scalogram ($\eta = 2\pi$ and $G_s = 5.336$) applied to the time waveform is presented in Fig. 8(b). The analysis properly represented the non-dispersive character of the signals throughout the 1000–9000 Hz. The result is better seen in the arrival time plots of Fig. 8(c) extracted from the scalogram ridges. The larger width of the GWT contours at the low frequencies is a necessary consequence of the uncertainty

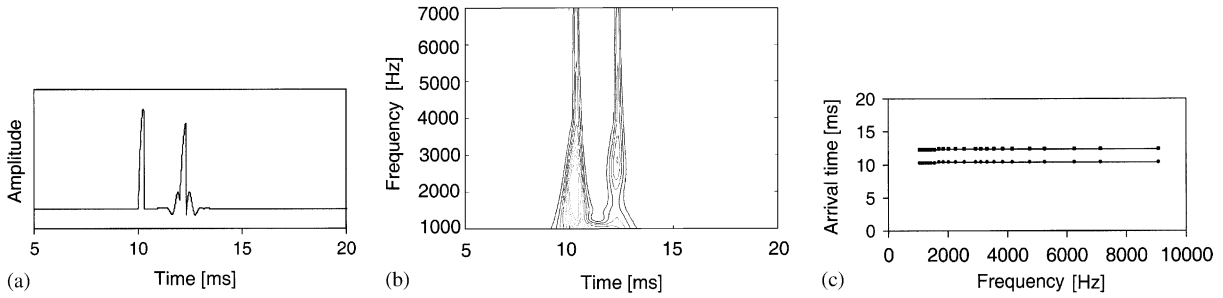

Fig. 8. (a) Simulated unfiltered and filtered pulses in the time domain. (b) Normalized Gabor wavelet scalogram of trace (a) with $\eta = 2\pi$ and $G_s = 5.336$. (c) Arrival times extracted from scalogram: •, unfiltered pulse; ▩, filtered pulse.

principle and it does not affect the determination of the energy arrival time (*positions* of the ridges of the contours). Fig. 8 also confirms that frequency-dependent attenuation does not affect the velocity measurements.

Excluding an analysis error in obtaining the dispersive behavior at the low frequencies in Fig. 7(a), one possible explanation is the occurrence of phase changes at the reflecting ends of the rail. As the rail section was cut manually with a blow torch, the end surfaces were not perfectly flat. This possibility is substantiated by noting that the dispersion seen in the echo signal is almost non-existent in the first arrival in Fig. 4(b).

The group velocities measured for the lateral and the vertical modes are shown in Fig. 7(b) together with the predictions of Ref. [2]. In this reference the two modes are denominated *fh* (flexural horizontal) and *fv* (flexural vertical) respectively. It can be seen, again, that the measurements agree qualitatively with the predictions. A general observation is that both the lateral and the vertical modes propagate at lower velocities than the longitudinal mode for frequencies below 5200 Hz. This behavior is expected given the lower propagation velocity of bending modes when compared to axial modes in prismatic waveguides at low frequencies. Moreover, the vertical mode is slightly faster than the lateral mode throughout the frequency range examined. The same trend was confirmed in previous analyses [2,3] and field measurements [7] on rails. The average measured velocity is 2 km/s for the vertical mode and 1.7 km/s for the lateral mode. Above 1 kHz, the vertical mode of a rail can be approximated to shear-dominated bending vibrations (Timoshenko beam) with nominal velocity equal to sqrt(G'/ρ) where the equivalent shear modulus G' is 0.4 times the shear modulus G. For $G = 82$ GPa and $\rho = 7800$ kg/m^3, the nominal vertical wave velocity is 2 km/s that matches exactly with the average measured value. Both the vertical mode and the lateral mode exhibit an appreciable dispersive behavior in Fig. 7(b). The group velocities generally increase with frequency for the lateral mode and exhibit a non-monotonic dependence on frequency for the vertical mode.

4.4. Frequency-dependent attenuation

The frequency-dependent attenuation values obtained from the GWT scalograms are presented in Fig. 9 for the longitudinal, the lateral and the vertical modes. Attenuation in these tests is primarily the result of energy losses in the sleeper supports with a minor contribution of material damping. The possibility for mode conversion at the reflecting ends as another possible cause of

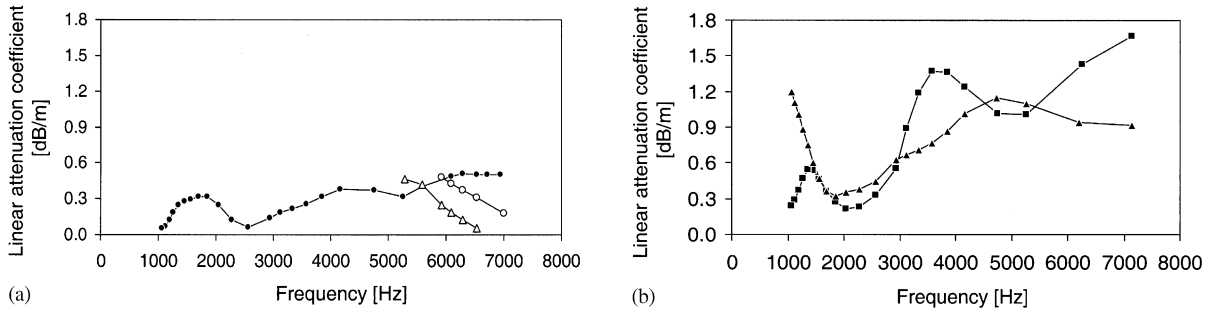

Fig. 9. (a) Linear attenuation coefficients for the longitudinal modes: •, lowest order mode L0; △, higher order mode L1; ○, higher order mode L2. (b) Linear attenuation coefficients for the lateral and for the vertical modes: ▩, vertical mode; ▲, lateral mode.

attenuation was eliminated as the scalogram contour patterns did not reveal the presence of mode-converted waves.

Attenuation values for the longitudinal modes in Fig. 9(a) are relatively small as expected in acoustic waveguides. The attenuation of mode L0 tends to increase with frequency above 2500 Hz reaching the maximum value of 0.5 dB/m at 7000 Hz. The attenuation minimum of 0.05 dB/m for this mode is found at 1000 and 2500 Hz. Contrarily to L0, the higher order modes L1 and L2 attenuate at a lower rate with increasing frequency from a maximum value of 0.47 dB/m measured at the respective cut-on frequencies of 5300 Hz for L1 and 5900 Hz for L2.

Comparing the data in Fig. 9(b) to those in Fig. 9(a), it is clear that the attenuation rates measured for the lateral and the vertical modes are generally larger than those of the longitudinal modes. This behavior is expected as the bending vibrations are more sensitive to damping in the supports than their longitudinal counterparts. Also from a material damping standpoint, shear-dominated waves are generally characterized by larger losses than longitudinal-type waves. The attenuation of the lateral mode is larger than that of the vertical mode below 3000 Hz; the opposite trend is observed above 3000 Hz with the exception of two measurement points. The minimum attenuation of 0.2 dB/m for the vertical mode is measured at 1000 and 2000 Hz. Above 2000 Hz, the attenuation for this mode generally increases with frequency reaching 1.7 dB/m at 7000 Hz. For the lateral mode, the minimum attenuation of 0.3 dB/m is found at 1850 Hz and losses stabilize at 0.9 dB/m at 7000 Hz. The attenuation values measured in Fig. 9(b) have the same order of magnitude as the decay rates obtained by other authors in the 0–5000 Hz range [4,19,20]. As a specific example, the lateral wave decay rates obtained in these previous works are typically upper bounded by 1 dB/m above 1000 Hz as seen in Fig. 9(b). The general increase of the attenuation with frequency is due to the increased participation of the rail feet to the vibration. Feet vibrations are strongly affected by the large damping in the supports as previously noted in Ref. [19].

5. Conclusions

This paper shows the use of a joint time–frequency analysis based on the wavelet transform to characterize high-frequency multimode and dispersive waves propagating in railroad tracks.

Wavelet transforms optimize the time–frequency resolution of dynamic measurements and, theoretically, only require a single excitation point and a single detection point.

The Gabor wavelet transform was first applied to the flexural vibrations of a cylindrical waveguide for which exact theoretical solutions exist. This test showed the importance of the proper selection of the wavelet parameters for dispersive studies. A 4.6 m long section of 115 lb/yard AREA rail was then subject to impulse testing in the laboratory. Three longitudinal modes, one lateral mode and one vertical mode were successfully identified in the 1000–7000 Hz range by the joint time–frequency analysis. The group (energy) velocity dispersion curves and the frequency-dependent attenuation of the waves were obtained from the corresponding wavelet scalograms.

The measurements qualitatively agree with previous literature results of rail vibration studies. An unexpected dispersive behavior measured for the lowest order longitudinal mode was explained by possible phase changes occurring at the rail reflecting ends. The two higher order longitudinal modes cut on at 5300 and at 5900 Hz, respectively. The lateral and the vertical modes exhibit appreciable dispersion. Moreover, the lateral mode is always slower than the vertical mode and both modes are slower than the longitudinal mode below 5200 Hz.

The attenuation rates of transient vibrations in rails are generally low as expected in acoustic waveguides where beam spreading is minimized. Minimum attenuation is measured at 1000 and 2500 Hz for the lowest order longitudinal mode. The attenuation of the higher-order longitudinal modes decreases with increasing frequency from the maximum value of 0.47 dB/m occurring at the respective cut-on frequencies. The attenuation rates of the lateral and the vertical modes are generally larger than those of the longitudinal modes. Minimum attenuation is found at 1850 Hz for the lateral mode and at 1000 and 2000 Hz for the vertical mode. However, the absence of fasteners in the laboratory set-up examined in this work would make it difficult to extrapolate the attenuation results to the field.

Field testing will be performed in a subsequent phase of this research by using the same time–frequency analysis. Since a reflection from the rail end would not generally be available in the field, a pair of accelerometers could be used to exploit the advantages of the dual detection scheme. Although dual detection is advisable as discussed in Section 4.1, a single detection point is theoretically required to extract velocity and attenuation values once the excitation signal is well characterized.

Acknowledgements

This work was funded by the US National Science Foundation under Grant CMS-84249 and by the Department of Transportation under Federal Railroad Administration Grant DTFR53-02-G-00011. San Diego Trolley, Inc. is gratefully acknowledged for donating the rail section tested in this study and for exchanging useful technical discussions.

References

[1] D.J. Thompson, Wheel-rail noise generation, Part III: rail vibration, *Journal of Sound and Vibration* 161 (1993) 421–446.

[2] L. Gavric, Computation of propagative waves in free rail using a finite element technique, *Journal of Sound and Vibration* 185 (1995) 531–543.
[3] T.X. Wu, D.J. Thompson, A double Timoshenko beam model for vertical vibration analysis of railway track at high frequencies, *Journal of Sound and Vibration* 224 (1999) 329–348.
[4] T.X. Wu, D.J. Thompson, Analysis of lateral vibration behavior of railway track at high frequencies using a continuously supported multiple beam model, *Journal of the Acoustical Society of America* 106 (1999) 1369–1376.
[5] A. Nordborg, Wheel/rail noise generation due to nonlinear effects and parametric excitation, *Journal of the Acoustical Society of America* 111 (2002) 1772–1781.
[6] L. Gry, Dynamic modeling of railway track based on wave propagation, *Journal of Sound and Vibration* 195 (1996) 477–505.
[7] D.J. Thompson, Experimental analysis of wave propagation in railway tracks, *Journal of Sound and Vibration* 203 (1997) 867–888.
[8] D. Alleyne, P. Cawley, A two-dimensional Fourier transform method for the measurement of propagating multimode signals, *Journal of the Acoustical Society of America* 89 (1991) 1159–1168.
[9] K. Kishimoto, H. Inoue, M. Hamada, T. Shibuya, Time frequency analysis of dispersive waves by means of wavelet transform, *American Society of Mechanical Engineers Journal of Applied Mechanics* 62 (1995) 841–846.
[10] J. Jeon, Y.S. Shin, Pseudo Wigner–Ville distribution, computer program and its applications to time-frequency domain problems, Naval Postgraduate School Report NPS-ME-93-002, 1993.
[11] H. Inoue, K. Kishimoto, T. Shibuya, Experimental wavelet analysis of flexural waves in beams, *Experimental Mechanics* 36 (1996) 212–217.
[12] Y.Y. Kim, E.-H. Kim, Effectiveness of the continuous wavelet transform in the analysis of some dispersive elastic waves, *Journal of the Acoustical Society of America* 110 (2001) 86–94.
[13] S.-C. Wooh, K. Veroy, Spectrotemporal analysis of guided-wave pulse-echo signals. Part 2: numerical and experimental investigations, *Experimental Mechanics* 41 (2001) 332–342.
[14] H. Jeong, Y.-S. Jang, Wavelet analysis of plate wave propagation in composite laminates, *Composite Structures* 49 (2000) 443–450.
[15] Y. Hayashi, S. Ogawa, H. Cho, M. Takemoto, Non-contact estimation of thickness and elastic properties of metallic foils by the wavelet transform of laser-generated Lamb waves, *NDT&E International* 32 (1999) 21–27.
[16] L. Gaul, S. Hurlebaus, L.J. Jacobs, Localization of a "synthetic" acoustic emission source on the surface of a fatigue specimen, *Research in Nondestructive Evaluation* 13 (2001) 105–117.
[17] S. Mallat, *A Wavelet Tour of Signal Processing*, 2nd Edition, Academic Press, New York, 1999.
[18] A.H. Meitzler, Mode coupling occurring in the propagation of elastic pulses in wires, *Journal of the Acoustical Society of America* 33 (1961) 435–445.
[19] D.J. Thompson, N. Vincent, Track dynamic behavior at high frequencies. Part I: theoretical models and laboratory measurements, *Vehicle System Dynamics Supplement* 24 (1995) 86–99.
[20] D.J. Thompson, N. Vincent, Track dynamic behavior at high frequencies. Part II: experimental results and comparisons with theory, *Vehicle System Dynamics Supplement* 24 (1995) 100–114.